International Journal of Thermal Sciences 49 (2010) 319–332

Contents lists available at ScienceDirect

International Journal of Thermal Sciences

journal homepage: www.elsevier.com/locate/ijts

Forced convection in thermally developing region of a channel partially filled with a porous material and optimal porous fraction

V.V. Satyamurty [a,*], D. Bhargavi [b,1]

[a] Dept. of Mech. Engg., Indian Institute of Technology, Kharagpur, West Bengal 721302, India
[b] Dept. of Mathematics, Indian Institute of Technology, Kharagpur 721302, India

ARTICLE INFO

Article history:
Received 8 May 2009
Received in revised form
6 July 2009
Accepted 28 July 2009
Available online 21 August 2009

Keywords:
Channels partially filled with porous material
Optimal porous insert
Heat transfer enhancement

ABSTRACT

Local Nusselt numbers have been obtained on the porous side and the fluid side of the parallel plate channel. Plots to obtain wall heat transfer directly have been presented. Change in wall heat transfer has been examined to establish that the maximum enhancement in heat transfer occurs at a porous fraction of 0.8 at a Darcy number of 0.001. Correspondingly, the maximum enhancement per unit pressure drop occurs at a porous fraction of 0.7. As Darcy number increases, the porous fraction at which the maximum enhancement in heat transfer occurs decreases.

1. Introduction

Forced convective Nusselt number is higher when ducts in general have been filled with porous material. For example, the fully developed Nusselt number for flow between parallel plates subjected to constant, equal temperatures is 7.53, see, p. 155, Shah and London [1], while the corresponding value when the channel is filled with a porous material is 9.27 (Kaviany [2], Poulikakos and Kazmierczak [3], Satyamurty and Marpu [4]) when the Darcy number, $Da = 0.001$. However, the increase in heat transfer is followed by increased pressure drop. In view of this and also because of present day applications, considerable attention is paid to study heat transfer in channels partially filled with porous materials. Recent applications, where studies on partially filled porous channels can be gainfully employed, include solar absorbers, catalytic and inert packed bed reactors, fuel cells, and in general compact heat exchangers. A typical proton exchange membrane (PEM) fuel cell consists of a gas channel, porous media gas diffuser, porous catalyst layer and a membrane. The internal flow configurations that are commonly studied are, the parallel plate channels or annuli or pipes with a central porous core or annular insert. However, from practical considerations, attaching the porous insert to one wall, may be the requirement of the device or may be of manufacturing of convenience.

Several studies examined the boundary conditions at the porous–fluid interface. Beavers and Joseph [5] first proposed the boundary conditions at the porous–fluid interface based on experimental investigation. Comprehensive literature survey on this subject is given in the monograph by Nield and Bejan [6]. Poulikakos and Kazmierczak [3] presented an exact solution of the forced convection in a channel, subjected to uniform heat flux and constant temperature at the walls, partly (symmetric) filled with a porous medium adjacent to both the walls using the non-Darcy–Brinkman model. Vafai and Kim [7] employed continuity of velocity and velocity gradients at the interface in obtaining an exact solution for fully developed flow, between a plate and an unbounded porous medium. Jang and Chen [8] have presented a numerical study of fully developed forced convection for the same configuration employing Darcy–Brinkman–Forchheimer model and included thermal dispersion effects in the porous matrix. Ochoa-Tapia and Whitaker [9,10] developed a boundary condition that accommodates a jump in the velocity gradients at the interface by applying volume-averaging technique. Subsequently this boundary condition commonly got referred to as stress jump boundary condition. Kuznetsov [11–14] extensively used the stress jump boundary condition and obtained analytical solutions for fluid flow

* Corresponding author. Tel.: +91 3222 282974; fax: +91 3222 282278
E-mail addresses: vvsmurty@mech.iitkgp.ernet.in (V.V. Satyamurty), bhargavi.math@gmail.com (D. Bhargavi).
[1] Tel: +91 3222 282974; fax: +91 3222 255303.

1290-0729/$ – see front matter © 2009 Elsevier Masson SAS. All rights reserved.
doi:10.1016/j.ijthermalsci.2009.07.023

Nomenclature

C_p	specific heat, J/(kg K)
Da	Darcy number, $(=K/H^2)$
H	spacing between the two plates, m
K	permeability of the medium, m^2
k_{eff}	effective thermal conductivity in the porous region, W/(m K)
k_f	thermal conductivity of the fluid, W/(m K)
l_p	thickness of the porous layer, m
MD	number of grids along the axial direction in the numerical scheme
$\dot{m}$	mass flow rate, kg/s
ND	number of grids in the normal (Y) direction
Nu_{1x}	local Nusselt number at wall 1 at $Y=-1/2$ for $0<\gamma_p<1.0$
Nu_{2x}	local Nusselt number at wall 2 at $Y=1/2$ for $0<\gamma_p<1.0$
$Nu^{\gamma_p=0}$	local Nusselt number for the clear fluid i.e., $\gamma_p=0$
$Nu^{\gamma_p=0}$	local Nusselt number for the channel fully filled with the porous material, i.e., $\gamma_p=1$
p	pressure, N/m^2
P_{gr}	non-dimensional pressure gradient, dP/dX
Pe	Peclet number, $(u_{ref}H)/\alpha_f$
Q_{xf}	energy gained by the fluid, defined by Eq. (34), J/(m s)
$\overline{Q}_{xf}$	non-dimensional energy gain by the fluid, defined by Eq. (35)
$\overline{Q}_{xw}$	non-dimensional total heat transfer from both the walls up to X^* for the channel partially filled with the porous material
$\overline{Q}_{xw}^{\gamma_p=0}$	non-dimensional total heat transfer from one wall up to X^* in the clear fluid channel i.e., when there is no porous insert, $\gamma_p=0$
$\overline{Q}_{xw}^{\gamma_p=1.0}$	non-dimensional wall heat transfer from one wall up to X^* in the channel fully filled with the porous material i.e., $\gamma_p=1.0$
$\overline{Q}_{xw1}$	non-dimensional wall heat transfer from wall 1 at $Y=-1/2$ up to X^* for the channel partially filled with the porous material
$\overline{Q}_{xw2}$	non-dimensional wall heat transfer from wall 2 at $Y=-1/2$ up to X^* for the channel partially filled with the porous material
T_b	bulk mean temperature, K
T_{bx}	suffix x is included to emphasize that T_b is at an axial distance of x in Eq. (34)
T_e	fluid inlet temperature at entry to the channel, K
T_f	temperature in the fluid region, K
T_p	temperature in the porous region, K
T_w	wall temperature, K
U_f	non-dimensional velocity in X direction in the fluid region $(=u_f/u_{ref})$
U_i	non-dimensional interfacial velocity
U_p	non-dimensional velocity in X direction in the porous region $(=u_p/u_{ref})$
u	velocity in x direction, m/s
u_f	velocity in the fluid region, m/s
u_p	velocity in the porous region, m/s
u_{ref}	reference velocity, m/s
X	non-dimensional axial coordinate
X^*	X/Pe
X^*_{fd}	value of X^* for the thermal field to be fully developed
x	dimensional coordinate in the flow direction
Y	non-dimensional coordinate in the normal direction to the flow
y	dimensional coordinate in the normal direction to the flow

Greek Symbols

α_f	thermal diffusivity of the fluid, m^2/s
α_{eff}	effective thermal diffusivity of the porous region, m^2/s
β	stress jump coefficient
γ_p	porous fraction, i.e., non-dimensional thickness of the porous layer, l_p/H
ΔNu	net change in Nusselt number defined by Eq. (41)
$\Delta\overline{Q}_{xw}$	net change in wall heat transfer defined by Eq. (39)
$\Delta\overline{Q}_{xw-PD}$	net change in wall heat transfer per unit pressure drop defined by Eq. (40)
ΔX^*	grid size in the axial direction $=X^*_{fd}/MD$
ΔY	grid size in the normal direction $=1/ND$
ε	μ_f/μ_{eff}
η	k_f/k_{eff}
θ_b	non-dimensional temperature based on bulk mean temperature
θ_f	non-dimensional temperature in the fluid region, $(T_f-T_w)/(T_e-T_w)$
θ_p	non-dimensional temperature in the porous region, $(T_p-T_w)/(T_e-T_w)$
θ^*	non-dimensional bulk mean temperature, $(T_b-T_w)/(T_e-T_w)$
μ_f	fluid dynamic viscosity, kg/(m s)
μ_{eff}	effective viscosity in the porous region, kg/(m s)

in channels partially filled with a porous medium. These investigations by Kuznetsov differ in the flow model employed to describe the porous region. Alazmi and Vafai [15] examined in detail the influence of different conditions at porous–fluid interface. Studies by Al-Nimr and Alkam [16], Chikh et al. [17] deal with heat transfer in annular ducts. Alkam and Al-Nimr [18,19], have employed porous substrates in solar collectors to improve the thermal performance.

Alkam et al. [20] examined the efficacy of depositing a given amount of porous material on one wall compared to distributing on both the walls of the channel on enhancement of heat transfer. The channel walls were subjected to constant temperature. Alkam et al. concluded that the enhancement in heat transfer is higher when the porous material is distributed equally on the two walls when the porous fraction is low, while depositing on one wall is advantageous for high porous fractions. Further, the pressure gradient has been found to be higher when the porous material is deposited on one wall only for all porous fractions. Hamdan et al. [21] stated that the maximum Nusselt number is achieved when the porous insert of certain thickness is placed at the middle of the channel. However, explicit evaluation of the optimum thickness or dependence of enhancement in Nusselt number on the porous insert thickness has not been brought out. Bhargavi et al. [22] very recently studied the effect of porous fraction and interfacial stress jump on fully developed skin friction and heat transfer in flow through a channel partially filled with porous material. The channel walls are subjected to uniform heat flux. Bhargavi et al. showed that the net change in the Nusselt numbers at the two walls though, is negative for small porous fractions, becomes positive and for some porous fraction (<1), even exceeds the change that follows when the channel is fully filled with porous material. Further, Bhargavi et al.

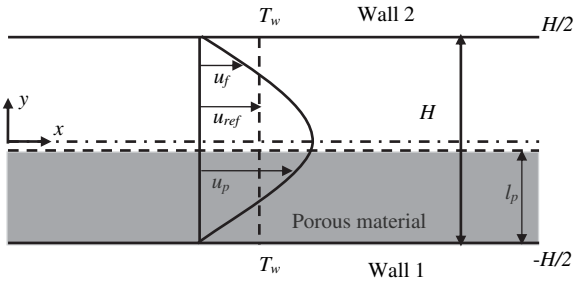

Fig. 1. Physical model and the coordinate system.

noted that the contribution from the fluid side to the change in the Nusselt number is more significant. Thus the trends, reported in Bhargavi et al. support the conclusion of Hamdan et al. since the channel with a porous core has two fluid filled regions. It is noted that the thermal boundary conditions employed in Bhargavi et al. and in Alkam et al. and Hamdan et al. are different. Also, the conclusion of Alkam et al. [20] is based on the ratio of accumulated heat transferred in the two arrangements considered, whereas the pressure drop is a point function. Even though Alkam et al.'s investigation determines the better of the two arrangements of the porous insert vis-à-vis the porous layer thickness, does not address the basic issue, whether the porous insert enhances the heat transfer at all compared to heat transfer in a clear channel.

The present investigation is taken up to establish the condition for heat transferred in the porous insert added channel is higher than that compared to the clear channel and determine the optimum thickness of the porous material when attached to one wall only. The channel walls are subjected to equal, constant temperature. The flow in both the regions is assumed to be fully developed and the thermal field is developing. The study establishes the optimum thickness based for the maximum enhancement in the cumulative heat transfer as well as cumulative heat transfer per unit pressure drop.

2. Mathematical formulation

The physical model and the coordinate system, that of a channel formed by parallel plates, H distance apart, partially filled with a porous insert attached to one wall is shown in Fig. 1. x is the axial distance and y is normal to the flow direction measured from the center line of the channel. As per the coordinate system, the plates are at $y = \pm H/2$. The plate at $y = -H/2$ shall be referred to as wall 1 and the plate at $y = H/2$ as wall 2.

The thickness of the porous material is l_p. The porous material of thickness l_p is adjacent to the wall 1 as shown in Fig. 1. The fluid enters at a temperature of T_e. Both the walls are subjected to uniform temperature of T_w. The problem has been studied under the assumptions, that the flow is steady, incompressible and fully developed. The fluid and the porous matrix are in local thermal equilibrium. The porous medium is homogeneous and isotropic. Pressure work is neglected and the fluid properties are assumed to be constant. The flow in both the porous and clear fluid regions is assumed to be fully developed, as obtained from Brinkman extended non-Darcy model and Hagen–Poiseuille flow with relevant boundary conditions at the walls and at fluid–porous interface. The following non-dimensional variables have been introduced.

$$X = \frac{x}{H},\ Y = \frac{y}{H},\ U_{f,p} = \frac{u_{f,p}}{u_{ref}},\ P = \frac{p}{\mu_f H u_{ref}/K},$$
$$\theta_{f,p} = \frac{T_{f,p} - T_w}{T_e - T_w} \tag{1}$$

In Eq. (1), X, Y are the non-dimensional axial and normal coordinates. U and P are the non-dimensional velocity, and pressure. The corresponding dimensional velocity and pressure are u and p. u_{ref} used to non-dimensionalize velocity, is the average velocity through the channel which can be obtained from the volumetric flow rate per unit width of the channel or by averaging the velocities in the fluid and porous regions. θ is the non-dimensional temperature. The subscripts f and p refer to the fluid and porous regions. μ_f is the viscosity of the fluid, K is the permeability of the porous medium and k_f is the thermal conductivity of the fluid. In addition, the non-dimensional porous layer thickness γ_p, referred to as porous fraction, is defined by,

$$\gamma_p = l_p/H \tag{2}$$

The governing equations for conservation of momentum and energy applicable in the fluid and porous region in non-dimensional form are as following.

Fluid Region:

$$0 = -\frac{dP}{dX} + Da\frac{d^2U_f}{dY^2} \tag{3}$$

$$U_f\frac{\partial\theta_f}{\partial X^*} = \frac{\partial^2\theta_f}{\partial Y^2} \tag{4}$$

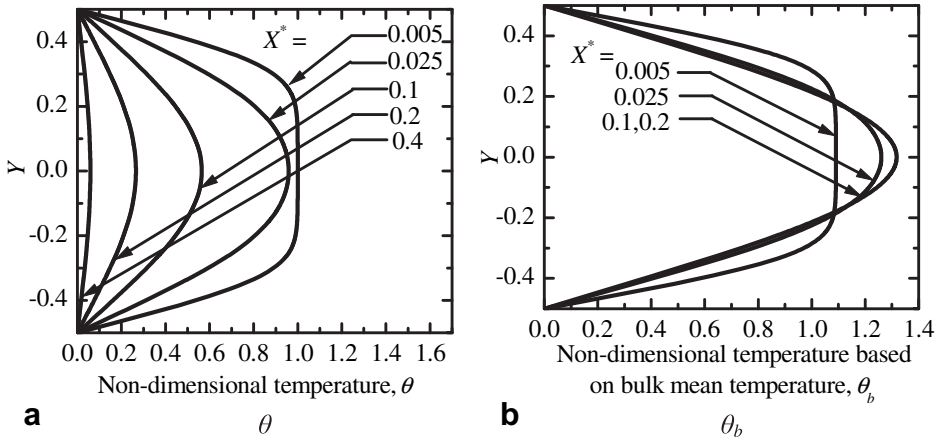

Fig. 2. Variation of (a) Non-dimensional temperature, θ and (b) Non-dimensional temperature based on bulk mean temperature, θ_b with Y at different axial positions for $\gamma_p = 0$.

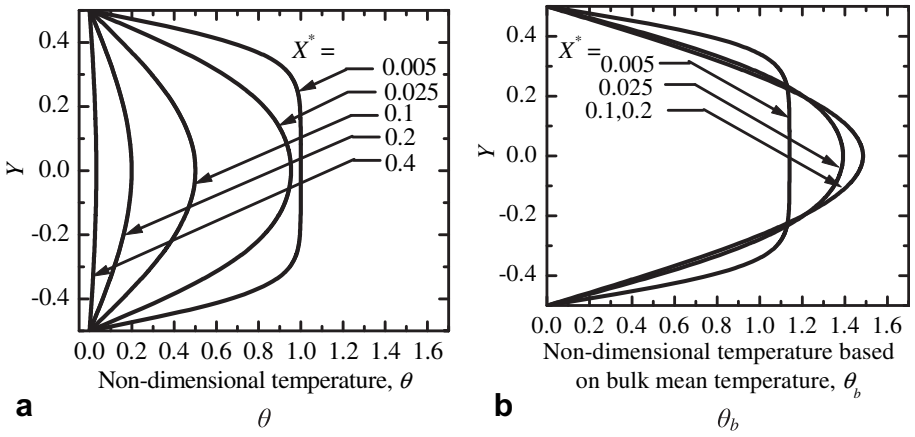

Fig. 3. Variation of (a) Non-dimensional temperature, θ and (b) Non-dimensional temperature based on bulk mean temperature, θ_b with Y at different axial positions for $\gamma_p = 1.0$ and $Da = 0.001$.

X^*, the normalized X, that rendered Eq. (4) independent of the Peclet number, Pe. X^* is defined by,

$$X^* = X/Pe \tag{5}$$

where

$$Pe = u_{ref}H/\alpha_f \tag{6}$$

In Eq. (3), Da, the Darcy number is defined by,

$$Da = K/H^2 \tag{7}$$

Porous Region:

$$U_p = -\frac{dP}{dX} + \frac{Da}{\varepsilon}\frac{d^2U_p}{dY^2} \tag{8}$$

$$U_p\frac{\partial\theta_p}{\partial X^*} = \frac{1}{\eta}\frac{\partial^2\theta_p}{\partial Y^2} \tag{9}$$

In Eqs. (8) and (9), ε and η are defined by,

$$\varepsilon = \mu_f/\mu_{eff} \quad \text{and} \quad \eta = \alpha_f/\alpha_{eff} = k_f/k_{eff} \tag{10}$$

Boundary conditions:

$$\theta_{f,p}(0,Y) = 1 \quad \text{at } X^* = 0 \text{ for } -1/2 \le Y \le 1/2 \tag{11}$$

$$U_p = 0, \quad \theta_p = 0 \quad \text{at } Y = -1/2 \quad \text{for } X^* > 0 \tag{12}$$

$$U_f = 0, \quad \theta_f = 0 \quad \text{at } Y = 1/2 \quad \text{for } X^* > 0 \tag{13}$$

$$U_p = U_f = U_i, \ \frac{1}{\varepsilon}\frac{dU_p}{dY} - \frac{dU_f}{dY} = \frac{\beta}{\sqrt{Da}}U_i \quad \text{at the interface, } Y = \gamma_p - 1/2 \tag{14}$$

$$\theta_p = \theta_f, \ \frac{\partial\theta_p}{\partial Y} = \eta\frac{\partial\theta_f}{\partial Y} \quad \text{at the interface, } Y = \gamma_p - 1/2 \quad \text{for } X^* > 0 \tag{15}$$

The conditions given in Eq. (14) ensure the continuity of the velocity and account for jump in the shear stress as given by Ochoa-Tapia and Whitaker [9] and [10] at the interface. In Eq. (14), β is the stress jump coefficient, which permits the necessary flexibility in the conditions to suit, say, experimental data.

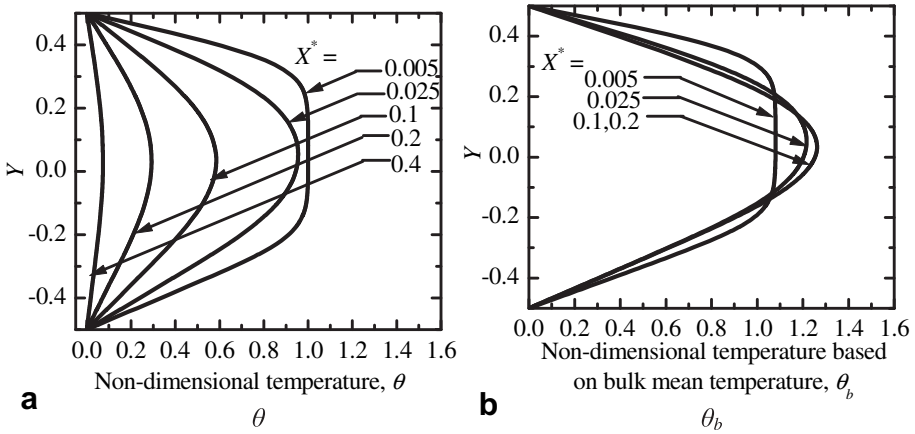

Fig. 4. Variation of (a) Non-dimensional temperature, θ and (b) Non-dimensional temperature based on bulk mean temperature, θ_b with Y at different axial positions for $\gamma_p = 0.2$ and $Da = 0.001$.

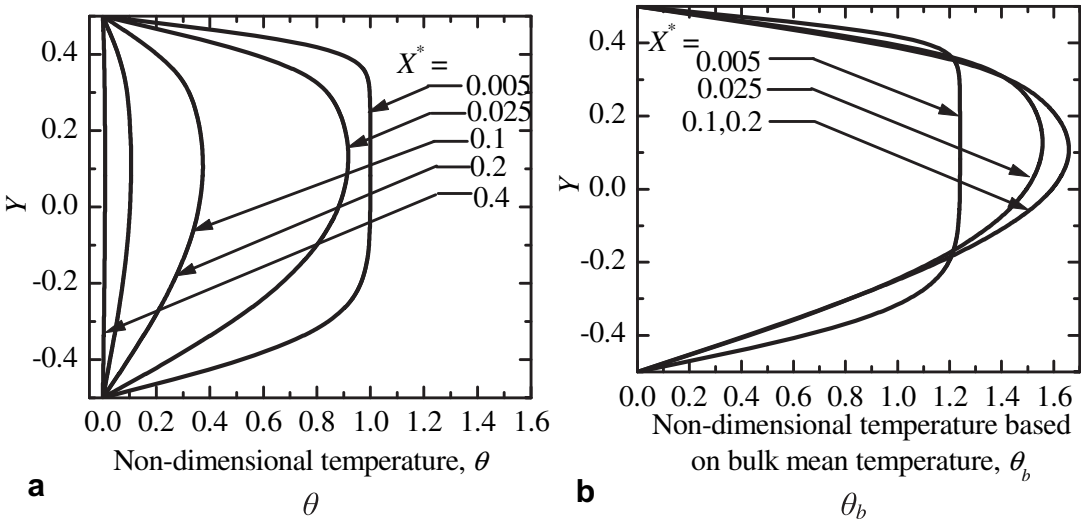

Fig. 5. Variation of (a) Non-dimensional temperature, θ and (b) Non-dimensional temperature based on bulk mean temperature, θ_b with Y at different axial positions for $\gamma_p = 0.8$ and $Da = 0.001$.

3. Expressions for velocity

3.1. Velocity profiles

On solving Eq. (3) along with the boundary conditions given by Eqs. (13) and (14), velocity in the fluid region is obtained as,

$$U_f(Y) = \frac{(2Y-1)\left[P_{gr}\left(1+2\left(Y-\gamma_p\right)\right)\left(\gamma_p-1\right)+4DaU_i\right]}{8Da\left(\gamma_p-1\right)} \tag{16}$$

where $P_{gr} = dP/dX$, is the pressure gradient.

Similarly, on solving Eq. (8), along with the boundary conditions given by Eqs. (12) and (14), velocity in the porous region is given by,

$$U_p(Y) = \frac{1}{2}\left(-1+\frac{\omega_2}{\omega_1}\right)\left(-1+e^{\frac{(1+2Y)\sqrt{\varepsilon}}{2\sqrt{Da}}}\right)e^{-Y\sqrt{\frac{\varepsilon}{Da}}}\left[A_1\left(P_{gr}+U_i\right)\times\left(e^{-\frac{1}{2}\sqrt{\frac{\varepsilon}{Da}}}-e^{Y\sqrt{\frac{\varepsilon}{Da}}}\right)-p_{gr}\left(e^{Y\sqrt{\frac{\varepsilon}{Da}}}+A_2e^{-\frac{1}{2}\sqrt{\frac{\varepsilon}{Da}}}\right)\right] \tag{17}$$

where

$$\omega_1 = \sinh\left[\gamma_p\sqrt{\varepsilon/Da}\right] \tag{18}$$

$$\omega_2 = \cosh\left[\gamma_p\sqrt{\varepsilon/Da}\right] \tag{19}$$

$$A_1 = \omega_1+\omega_2 \tag{20}$$

$$A_2 = 1+2\omega_1A_1 \tag{21}$$

U_i, the interfacial velocity in Eqs. (16) and (17) is determined from the stress jump condition in Eq. (14) as,

$$U_i = \frac{6(A_1-1)\sqrt{Da\varepsilon}\left(\gamma_p-1\right)\left[2(A_1-1)\sqrt{Da}-(A_1+1)\left(\gamma_p-1\right)\sqrt{\varepsilon}\right]}{\left\{\begin{array}{l}12(A_1-1)Da^{3/2}\left\{2(A_1-1)\sqrt{Da\varepsilon}-\left[(A_1+1)\left(\gamma_p-1\right)+2(1-A_1)\beta\left(\gamma_p-1\right)\sqrt{\varepsilon}+(A_1+1)\gamma_p\varepsilon\right]\right\}\\+\left(\gamma_p-1\right)^3\sqrt{\varepsilon}\left[4(A_2-1)\sqrt{Da\varepsilon}+\left(A_2\left(\beta\sqrt{\varepsilon}-1\right)-\left(1+\beta\sqrt{\varepsilon}\right)\right)\right]+12Da\left(\gamma_p-1\right)\sqrt{\varepsilon}\left[A_2\left(\beta\sqrt{\varepsilon}-1\right)-\left(1+\beta\sqrt{\varepsilon}\right)-2A_1\left(\gamma_p-1\right)\right]\end{array}\right\}} \tag{22}$$

P_{gr}, the non-dimensional pressure gradient is determined from,

$$\int_{-1/2}^{\gamma_p-1/2} U_p dY + \int_{\gamma_p-1/2}^{1/2} U_f dY = 1 \tag{23}$$

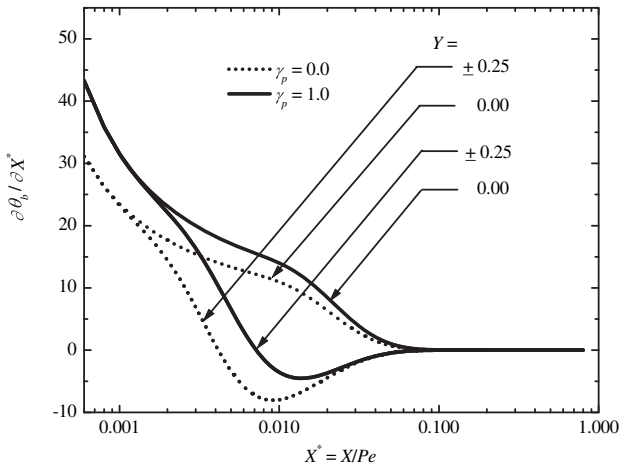

Fig. 6. Variation of $\partial\theta_b/\partial X^*$ with X^* for $\gamma_p = 0$ and $\gamma_p = 1.0$.

P_{gr} is given by,

$$P_{gr}=\frac{dP}{dX}=\frac{12\left[\left(1-\gamma_p\right)(1+A_2)+\left[\sqrt{Da}+\beta\left(\gamma_p-1\right)\right]\sqrt{\varepsilon}(A_2-1)\right]}{\left\{\begin{array}{l}12(A_1-1)Da^{3/2}\left\{2(A_1-1)\sqrt{Da\varepsilon}-\left[(A_1+1)\left(\gamma_p-1\right)+2(1-A_1)\beta\left(\gamma_p-1\right)\sqrt{\varepsilon}+(A_1+1)\gamma_p\varepsilon\right]\right\}\\+\left(\gamma_p-1\right)^3\sqrt{\varepsilon}\left[4(A_2-1)\sqrt{Da\varepsilon}+\left(A_2\left(\beta\sqrt{\varepsilon}-1\right)-\left(1+\beta\sqrt{\varepsilon}\right)\right)\right]+12Da\left(\gamma_p-1\right)\sqrt{\varepsilon}\left[A_2\left(\beta\sqrt{\varepsilon}-1\right)-\left(1+\beta\sqrt{\varepsilon}\right)-2A_1\left(\gamma_p-1\right)\right]\end{array}\right\}} \tag{24}$$

The details of the procedure and the expressions for U_f, U_p and P_{gr} given by Eqs. (16), (17) and (24) are available in Bhargavi et al. [22].

4. Numerical scheme: SAR

Numerical solutions to Eqs. (4) and (9) along with the boundary conditions on θ given in Eqs. (11–15) have been obtained employing the Successive Accelerated Replacement (SAR) scheme as described in Satyamurty [23] and used extensively in [24–30]. The basic philosophy of the SAR scheme is to guess a profile for each variable that satisfies the boundary conditions. Let the partial differential equation governing a variable, $\phi(x,y)$, expressed in finite difference form be given by $\overline{\phi}_{M,N} = 0$ where (M, N) represent the nodal point, when the non-dimensional height and length of the channel are divided into a finite number of intervals MD, ND respectively. The guessed profile for the variable ϕ at any mesh point, in general, will not satisfy the equation. Let the error in the equation at (M, N) and kth iteration be $\overline{\phi}^k_{M,N}$. The $(k+1)$th approximation to the variable ϕ is obtained from,

$$\phi^{k+1}_{M,N} = \phi^k_{M,N} - \omega\left\{\overline{\phi}^k_{M,N}/\left(\partial\overline{\phi}^k_{M,N}/\partial\phi_{M,N}\right)\right\} \tag{25}$$

In Eq. (25), ω is an acceleration factor which varies between $0 < \omega < 2$. $\omega < 1$ represents under relaxation and $\omega > 1$ represents over relaxation. The procedure of correcting the variable ϕ at each mesh point in the entire region of interest is repeated until a convergence criterion is satisfied. The criterion is that, the normalized change in the variable at any mesh point between kth and $(k+1)$th approximation satisfies,

$$\left|1-\left(\phi^k_{M,N}/\phi^{k+1}_{M,N}\right)\right| < \varepsilon \tag{26}$$

where ε, the error tolerance limit is a prescribed small positive number.

To correct the guessed profiles, each dependent variable has to be associated with one equation. It is natural to associate the equation for a variable that contains the highest order derivative of that variable. Non-dimensional temperatures θ_p and θ_f are corrected employing Eqs. (4) and (9).

4.1. Nusselt number

If h_{1x} and h_{2x} are the local heat transfer coefficients at the porous side wall (Wall 1) and fluid side wall (Wall 2), for a porous fraction of γ_p, the corresponding Nusselt numbers based on the hydraulic diameter are given by,

$$Nu_{1x} = \frac{h_{1x}(2H)}{k_f} = \frac{2}{\eta\theta^*}\left.\frac{\partial\theta}{\partial Y}\right|_{Y=-1/2} \tag{27}$$

$$Nu_{2x} = \frac{h_{2x}(2H)}{k_f} = -\frac{2}{\theta^*}\left.\frac{\partial\theta}{\partial Y}\right|_{Y=1/2} \tag{28}$$

θ^* in Eqs. (27) and (28) is the non-dimensional bulk mean temperature defined as,

$$\theta^* = \frac{T_b - T_w}{T_e - T_w} \tag{29}$$

In Eq. (29), T_b, the bulk mean temperature is defined by,

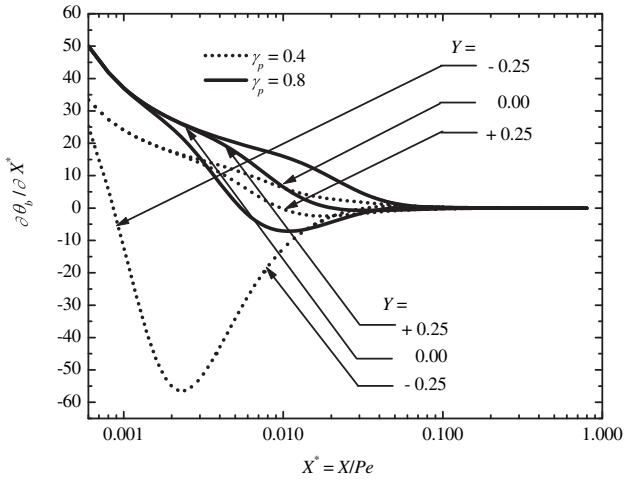

Fig. 7. Variation of $\partial\theta_b/\partial X^*$ with X^* for $\gamma_p = 0.4$ and $\gamma_p = 0.8$ at $Da = 0.005$.

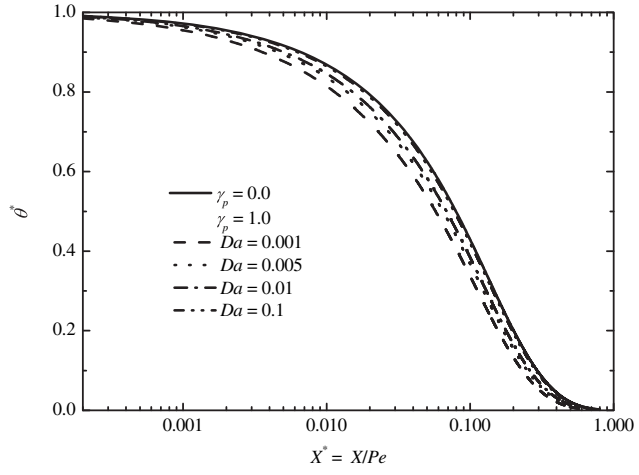

Fig. 8. Variation of non-dimensional bulk mean temperature θ^* with X^* for $\gamma_p = 0.0$ and 1.0.

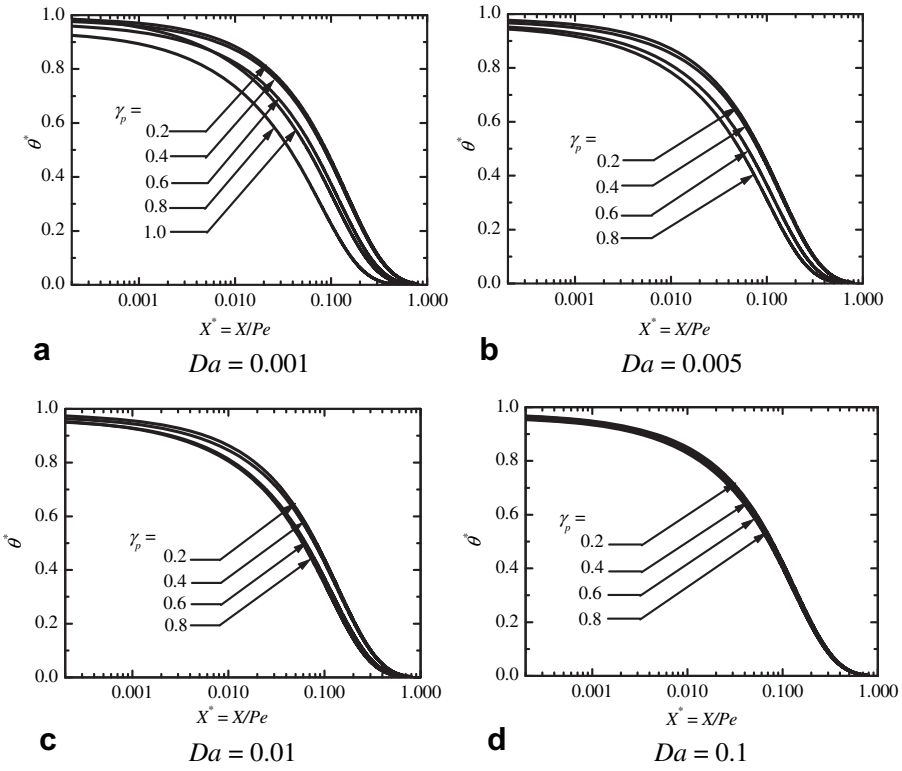

Fig. 9. Variation of non-dimensional bulk mean temperature θ^* with X^* for (a) $Da = 0.001$ (b) $Da = 0.005$ (c) $Da = 0.01$ and (d) $Da = 0.1$ for different porous fractions.

$$T_b = \frac{\int_{-H/2}^{l_p-H/2} u_p T_p dy + \int_{l_p-H/2}^{H/2} u_f T_f dy}{\int_{-H/2}^{l_p-H/2} u_p dy + \int_{l_p-H/2}^{H/2} u_f dy} \tag{30}$$

Using Eq. (30) in Eq. (29), the non-dimensional bulk mean temperature, θ^* can be expressed as,

$$\theta^* = \frac{\int_{-1/2}^{\gamma_p-1/2} U_p \theta_p dY + \int_{\gamma_p-1/2}^{1/2} U_f \theta_f dY}{\int_{-1/2}^{\gamma_p-1/2} U_p dY + \int_{\gamma_p-1/2}^{1/2} U_f dY} \tag{31}$$

It is also common to describe non-dimensional temperature based on bulk mean temperature defined by,

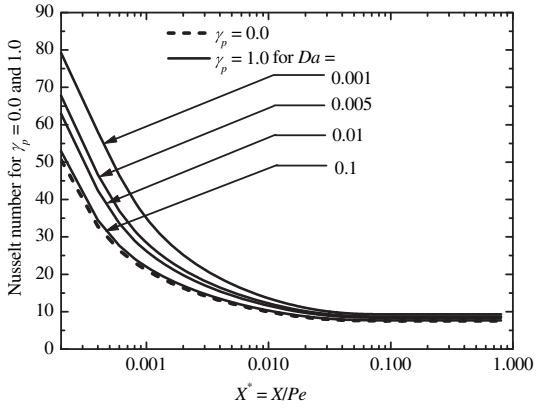

Fig. 10. Variation of Nusselt number with X^* for $\gamma_p = 0$ and $\gamma_p = 1.0$ for different Darcy numbers.

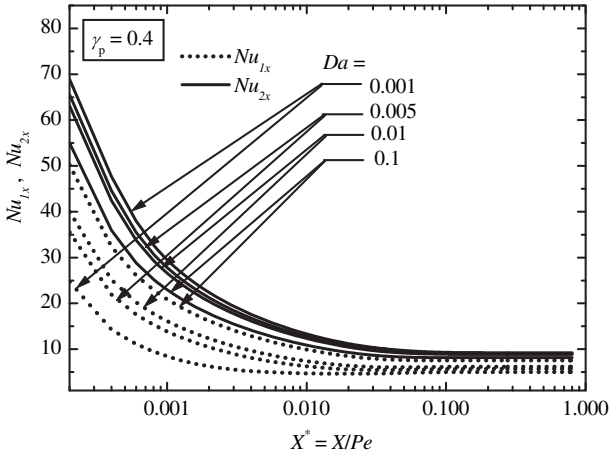

Fig. 11. Variation of Nusselt numbers Nu_{1x} and Nu_{2x} with X^* for $\gamma_p = 0.4$ at different Darcy numbers.

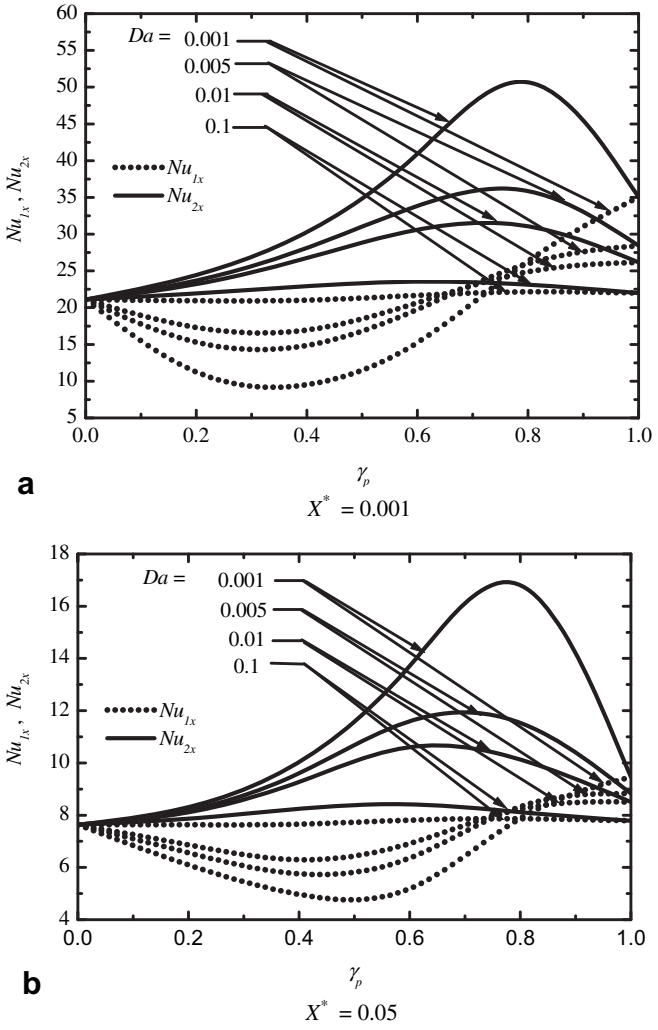

Fig. 12. Variation of Nusselt numbers Nu_{1x} and Nu_{2x} with γ_p at (a) $X^* = 0.001$ and (b) $X^* = 0.05$ for different Darcy numbers.

$$\theta_b = \frac{T - T_w}{T_b - T_w} \tag{32}$$

The familiar condition for the fully developed thermal field is expressed as,

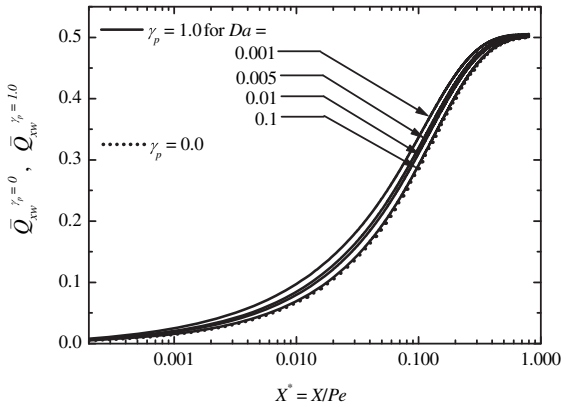

Fig. 13. Variation of $\overline{Q}_{xw}^{\gamma_p=0}$, $\overline{Q}_{xw}^{\gamma_p=1.0}$ with X^* for different Darcy numbers.

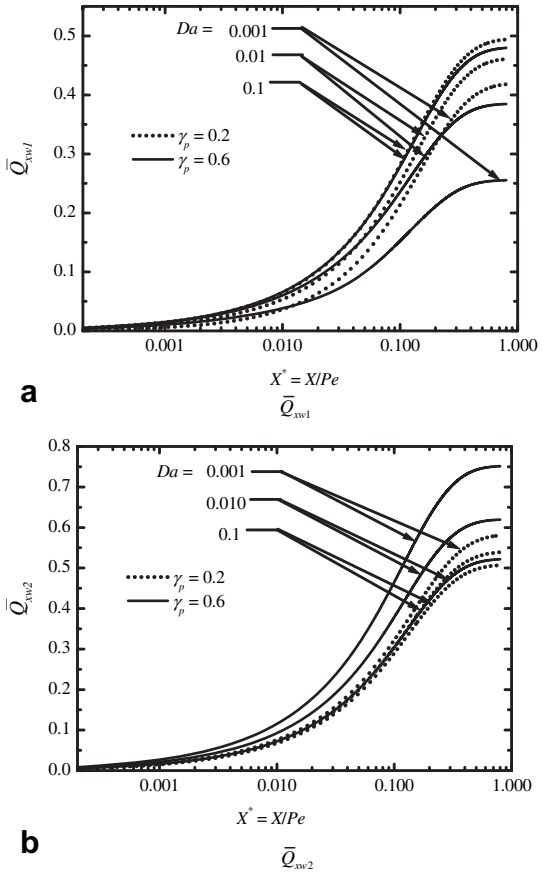

Fig. 14. Variation of (a) $\overline{Q}_{xw1}$ and (b) $\overline{Q}_{xw2}$ with X^* for $\gamma_p = 0.2$ and 0.6 for different Darcy numbers.

$$\frac{\partial \theta_b}{\partial X^*} = 0 \quad \text{for } X^* > X^*_{fd} \tag{33}$$

where X^*_{fd} is the axial normalized (with Peclet number) non-dimensional distance for the thermal filed to be fully developed. Eq. (33) need not be applied to Eqs. (4) and (9). Eq. (33), the standard condition for fully developed thermal field is given, to later on examine the validity when the channel is partially filled with the porous material as the geometric asymmetry lead to flow asymmetry.

5. Results and discussion

To implement the SAR scheme [23–30], X^*_{fd} has been chosen as 0.8. After numerical trials $\Delta X^* = 0.0001$ (corresponds to $MD = 4000$) and $\Delta Y = 0.025$ (corresponds to $ND = 40$) have been found to be satisfactory. The parabolic equations {Eqs. (4) and (9)} do not require imposition of downstream boundary condition, choice of ΔX^* alone is sufficient; however assigning $X^*_{fd} = 0.8$ is notional and sufficiently larger than the commonly reported values for clear fluid or fully filled with porous material channels. Non-dimensional temperature θ is corrected until the convergence criterion of $\varepsilon = 10^{-6}$ is satisfied between two successive iterations at all mesh points according to Eq. (26). Further, satisfactory convergence is obtained with $\omega < 1.0$, under relaxation. Under relaxation has become necessary owing to steep gradients in the velocity in the porous region, particularly for low Darcy number values.

Numerical solutions to Eqs. (4) and (9) have been obtained for $Da = 0.001$, 0.005, 0.01 and 0.1 for $\gamma_p = 0$, 0.2, 0.4, 0.6, 0.8 and 1.0

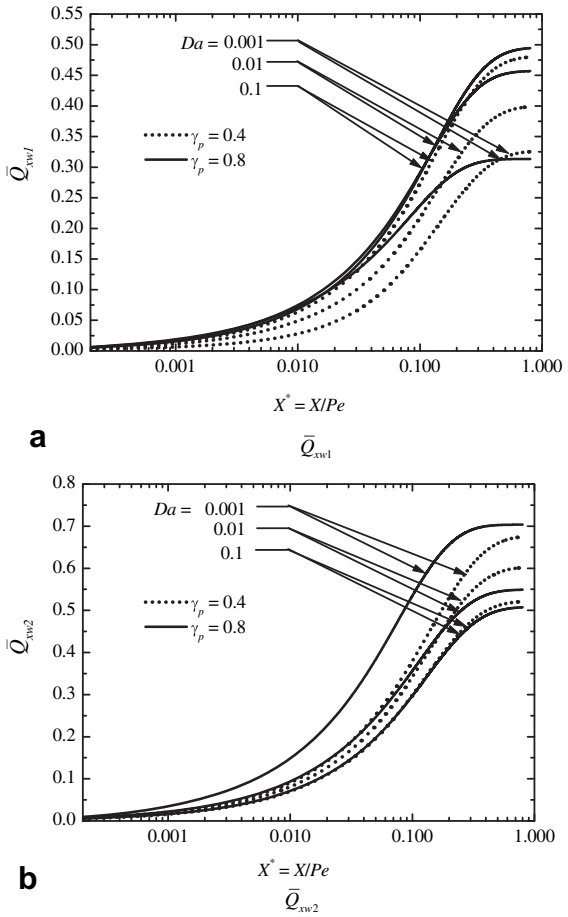

Fig. 15. Variation of (a) $\overline{Q}_{xw1}$ and (b) $\overline{Q}_{xw2}$ with X^* for $\gamma_p = 0.4$ and 0.8 for different Darcy numbers.

and assuming the stress jump coefficient $\beta = 0$. However, influence of the stress jump coefficient on Nusselt number has been examined for a selected value of, $Da = 0.001$, for $\gamma_p = 0.8$, where maximum changes in Nusselt number have been observed. Further, it has been assumed that $\varepsilon = \mu_f/\mu_{eff} = 1$ and $\eta = k_f/k_{eff} = 1$ throughout the computations. $\eta = k_f/k_{eff} = 1$ ensures that the expected enhancement in heat transfer is the least. $\eta < 1$ which is desirable for heat transfer enhancement leads to even higher enhancement in heat transfer.

5.1. Hydrodynamics

Hydrodynamics (velocity profiles, skin friction coefficient) and the influence of the stress jump coefficient are independent of the thermal field. Hydrodynamics, thus, remains the same as described in Bhargavi et al. [22].

5.2. Temperature profiles

Profiles of the non-dimensional temperature θ, and the non-dimensional temperature based on bulk mean temperature, θ_b, profiles are shown in Fig. 2(a) and (b) for $\gamma_p = 0$.

θ and θ_b profiles shown in Fig. 2(a) and (b) are the standard profiles for laminar forced convection through a parallel plate channel kept at constant temperature. For $X^* > 0.1$, θ_b is invariant, indicating fully developed condition. Similarly, θ and θ_b profiles shown in Fig. 3(a) and (b) for $\gamma_p = 1.0$ are the profiles for a channel fully filled with porous material, which are similar to those available in say, Mitrovic and Maletic [31] or Satyamurty and Marpu [4].

Profiles of θ, and θ_b for $Da = 0.001$, and the stress jump coefficient, $\beta = 0$, are shown in Fig. 4(a) and (b) for $\gamma_p = 0.2$ and in Fig. 5(a) and (b) for $\gamma_p = 0.8$, $Da = 0.001$, and $\beta = 0$. As can be expected, the profiles are not symmetric about $Y = 0$ as is the case for $\gamma_p = 0$ or $\gamma_p = 1.0$. As, X^* increases, $\theta \to 0$ for all Y, indicating no further heat transfer. Also, for large X^*, θ_b becomes invariant with X^*, indicating the onset of fully developed condition. However, this aspect is further elaborated by examining $\partial\theta_b/\partial X^*$ for different Y, in the clear fluid and porous regions.

5.3. Fully developed condition for thermal field

Plot of $\partial\theta_b/\partial X^*$ vs. X^* for $\gamma_p = 0$ and 1.0 at $Y = 0$ and $Y = \pm 0.25$ is shown in Fig. 6. $\partial\theta_b/\partial X^* \to 0$, for $X^* > 0.08$ which is the standard result {see, p. 172, Shah and London [1]} for $\gamma_p = 0$.

Similar plot for $\gamma_p = 0.4$ and 0.8 is shown in Fig. 7. It can be noticed from Fig. 7 that $\partial\theta_b/\partial X^*$ does go to zero for large $X^* > 0.15$. It is interesting to note for $\gamma_p = 0.4$ and 0.8, that $\partial\theta_b/\partial X^* \to 0$ at values of X^* higher than that for $\gamma_p = 0$ or 1.0. This is due to unequal rate of change in temperature in the axial direction in the porous and fluid regions, and the thermal field is considered as fully developed only after $\partial\theta_b/\partial X^* \to 0$ for all $-1/2 \le Y \le 1/2$.

5.4. Non-dimensional bulk mean temperature

Variation of θ^*, the non-dimensional bulk mean temperature, with X^* is shown in Fig. 8 for $\gamma_p = 0$ and $\gamma_p = 1.0$. θ^* decreases monotonically with X^*. For $\gamma_p = 1.0$, in addition, θ^* depends on Da, the Darcy number.

θ^* variation with X^* for $\gamma_p = 0.2$, 0.4, 0.6 and 0.8 is shown in Fig. 9(a–d) for $Da = 0.001$, 0.005, 0.01 and 0.1 respectively. Also shown in Fig. 9(a) is the variation of θ^* with X^* for $\gamma_p = 1.0$. Clearly, θ^* is neither maximum nor minimum for $\gamma_p = 1.0$, indicating the existence of an extremum value for $0 < \gamma_p < 1.0$. It can be seen from Fig. 9(a–d), as Da increases, the variation of θ^* with γ_p progressively decreases. This indicates that the flow in the porous region approaches the behavior of a clear fluid flow. This is in conformity with the characteristic displayed by channels fully filled with porous material for large Da.

5.5. Energy gain by the fluid

By making an energy balance on the fluid, energy gained by the fluid Q_{xf} up to x can be written as,

$$Q_{xf} = \dot{m} C_p (T_{bx} - T_e) \tag{34}$$

In Eq. (34), it may be noted that T_{bx} is nothing but the bulk mean temperature at an axial distance of x. The non-dimensional energy gain by the fluid, $\overline{Q}_{xf}$ is obtained, by dividing both sides of Eq. (34) with $\dot{m} C_p (T_w - T_e)$, as,

$$\overline{Q}_{xf} = 1 - \theta^* \tag{35}$$

From the plots given in Figs. 8 and 9, energy gained by the fluid up to a desired X^*, can be calculated. These plots can be used as an alternate to mean Nusselt number.

5.6. Nusselt number variation

In general, Nusselt number at the wall at $Y = -1/2$, i.e., adjacent to the porous material is designated as Nu_{1x} and as Nu_{2x}, at the wall at $Y = 1/2$, adjacent to the clear fluid. When $\gamma_p = 1.0$ or 0, $Nu_{1x} = Nu_{2x}$.

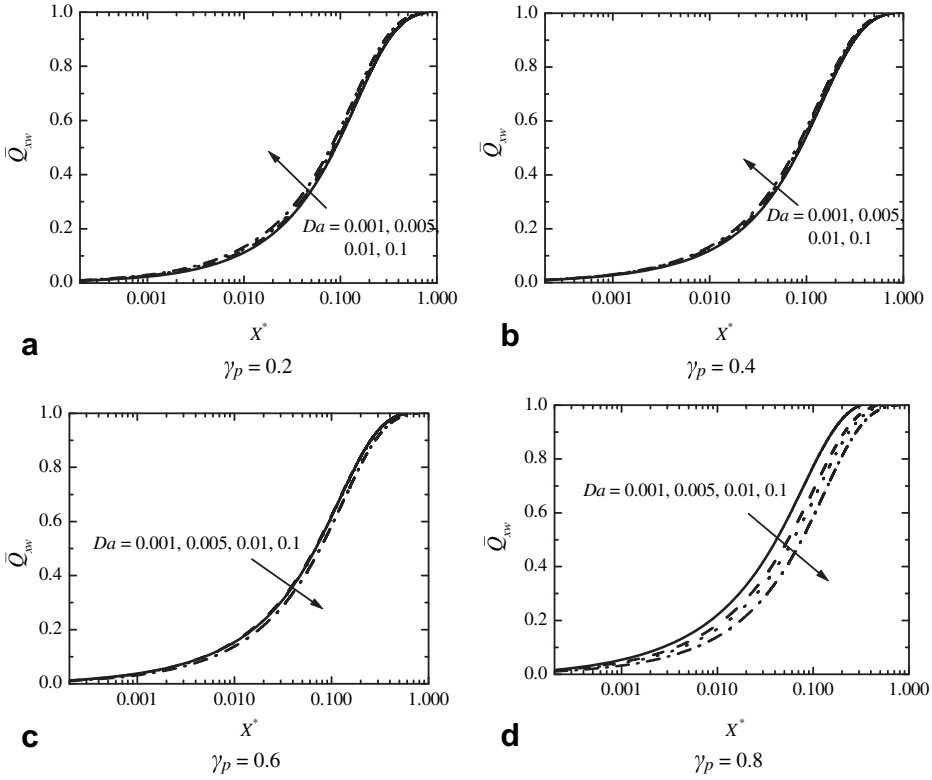

Fig. 16. Variation of $\overline{Q}_{xw}$ with X^*, for (a) $\gamma_p = 0.2$ (b) $\gamma_p = 0.4$ (c) $\gamma_p = 0.6$ and (d) $\gamma_p = 0.8$ for different Darcy numbers.

When $\gamma_p = 1.0$ the Nusselt number is designated as $Nu^{\gamma_p=1}$ and as $Nu^{\gamma_p=0}$ when $\gamma_p = 0$.

Variation of $Nu^{\gamma_p=1}$ and $Nu^{\gamma_p=0}$ with X^* is shown in Fig. 10. $Nu^{\gamma_p=1}$, depends on *Da*, whereas, $Nu^{\gamma_p=0}$ is independent of *Da*. $Nu^{\gamma_p=1} \rightarrow Nu^{\gamma_p=0}$ for high *Da*, say $\geq$0.1. $Nu^{\gamma_p=0}$ {=7.54, see, Shah and London, p. 155, [1]} and $Nu^{\gamma_p=1}$ reach the fully developed value for say, $X^* > 0.2$. The fully developed $Nu^{\gamma_p=1}$ values depend on the Darcy number and agree with the values reported in, say, Poulikakos and Kazmierczak [3].

Variation of Nu_{1x} and Nu_{2x} with X^* for $\gamma_p = 0.4$ is shown in Fig. 11 for different $Da = 0.001, 0.005, 0.01$ and 0.1. When $\gamma_p \neq 1$ or $\gamma_p \neq 0$, $Nu_{1x} \neq Nu_{2x}$ and both depend on the Darcy number owing to the coupling of the porous region and the clear fluid region. By comparing with the Nusselt number variations depicted in Fig. 11, with those in Fig. 10, it can be noted that $Nu_{1x}(\gamma_p = 0.4) < Nu^{\gamma_p=1}$ whereas, $Nu_{2x}(\gamma_p = 0.4) > Nu^{\gamma_p=0}$. Also, it can be noted that, $Nu_{1x} \rightarrow Nu_{2x} \rightarrow Nu^{\gamma_p=1} \rightarrow Nu^{\gamma_p=0}$ when *Da* is high, say, >0.1.

In order to examine the change in Nu_{1x} and Nu_{2x} with γ_p, plots of Nu_{1x} and Nu_{2x} vs. γ_p at fixed X^* have been made. Variation of Nu_{1x} and Nu_{2x} with γ_p for different $Da = 0.001, 0.005, 0.01$ and 0.1 for $\beta = 0$ is shown for fixed $X^* = 0.001$ and 0.05 in Fig. 12(a) and (b) respectively.

An interesting feature that can be noted from Fig. 12(a) and (b), is that, Nu_{2x} (the Nusselt number at the wall adjacent to the fluid region) is higher than $Nu^{\gamma_p=0}$ for all γ_p. It may be recalled that $Nu^{\gamma_p=0}$ is the Nusselt number for the clear fluid channel. Nu_{2x} displays a maximum for some $\gamma_p < 1.0$ and this value of γ_p decreases as *Da* increases. Whereas, Nu_{1x} (the Nusselt number at the wall adjacent to the porous) is lower than the $Nu^{\gamma_p=1}$ values for, say, $\gamma_p < 0.8$. Further, Nu_{1x} attains a minimum at some γ_p that decreases as *Da* increases. Contrasting variation of Nu_{1x} and Nu_{2x} with γ_p leads to the possibility of maximizing (or minimizing) the heat transfer from the walls by choosing an appropriate γ_p.

5.7. Wall heat transfer

In the present investigation, instead of the mean Nusselt number, a non-dimensional wall heat transfer is presented from which the heat transferred from the walls up to any desired X^* can be calculated conveniently. $\overline{Q}_{xw1}$, $\overline{Q}_{xw2}$ the non-dimensional heat transferred from the walls 1 and 2 at $Y-1/2$ and at $Y = 1/2$ respectively are defined by,

$$\overline{Q}_{xw1} = -\frac{\int_0^x k(\partial T/\partial y)|_{y=-H/2}\mathrm{d}x}{\dot{m}C_p(T_W - T_e)} = \int_0^{X^*} (\partial\theta/\partial Y)|_{y=-1/2}\mathrm{d}X^* \quad (36)$$

$$\overline{Q}_{xw2} = \frac{\int_0^x k(\partial T/\partial y)|_{y=H/2}\mathrm{d}x}{\dot{m}C_p(T_W - T_e)} = -\int_0^{X^*} (\partial\theta/\partial Y)|_{y=1/2}\mathrm{d}X^* \quad (37)$$

The total heat transferred from the two walls, $\overline{Q}_{xw}$ is given by,

$$\overline{Q}_{xw} = \overline{Q}_{xw1} + \overline{Q}_{xw2} \quad (38)$$

It may be noted that $\overline{Q}_{xw1} = \overline{Q}_{xw2}$ when $\gamma_p = 1.0$ or $\gamma_p = 0$ and are designated as $\overline{Q}_{xw}^{\gamma_p=1}$ and $\overline{Q}_{xw}^{\gamma_p=0}$ respectively.

Variation of non-dimensional wall heat transfers, $\overline{Q}_{xw}^{\gamma_p=1}$ and $\overline{Q}_{xw}^{\gamma_p=0}$ with X^* is shown in Fig. 13 by solid line for $\gamma_p = 1.0$ and by broken line for $\gamma_p = 0$. $\overline{Q}_{xw}^{\gamma_p=0}$ is independent of *Da* whereas $\overline{Q}_{xw}^{\gamma_p=1}$ depends on the Darcy number and decreases as *Da* increases. As can be expected, $\overline{Q}_{xw}^{\gamma_p=1} \rightarrow \overline{Q}_{xw}^{\gamma_p=0}$ for high, $Da > 0.1$. It may be noted that the total heat transferred from the two walls for $\gamma_p = 1.0$ or 0, is to be obtained as, $2\overline{Q}_{xw}^{\gamma_p=1}$ or $2\overline{Q}_{xw}^{\gamma_p=0}$.

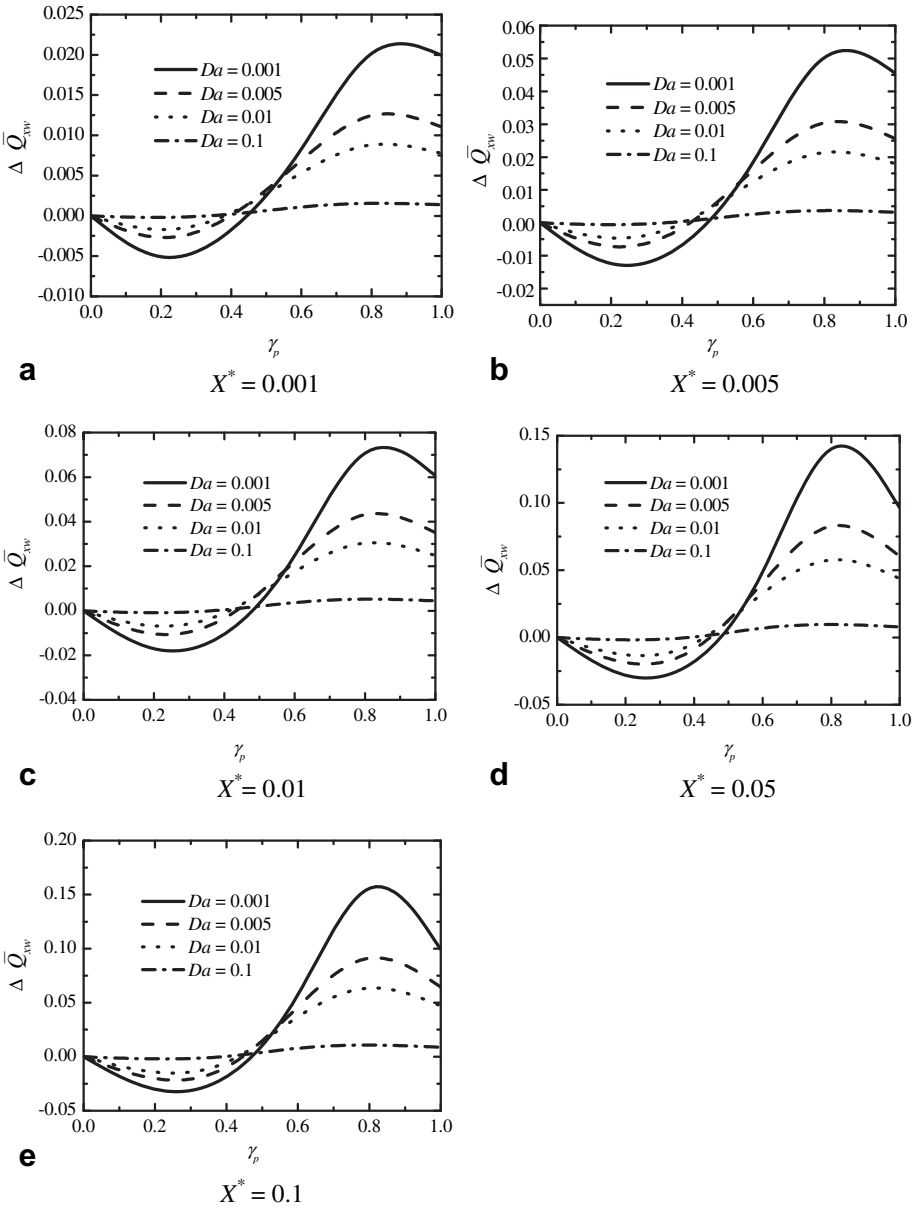

Fig. 17. Variation of $\Delta\overline{Q}_{xw}$ with γ_p for different Darcy numbers, at (a) $X^* = 0.001$, (b) $X^* = 0.005$, (c) $X^* = 0.01$, (d) $X^* = 0.05$ and (e) $X^* = 0.1$.

Variation of $\overline{Q}_{xw1}$ and $\overline{Q}_{xw2}$ with X^* is shown in Fig. 14(a) and (b) respectively for $\gamma_p = 0.2$, and 0.6 and in Fig. 15(a) and (b) for $\gamma_p = 0.4$, and 0.8. It is evident from Figs. 14 and 15 that, $\overline{Q}_{xw2} > \overline{Q}_{xw1}$ for a given *Da* and γ_p. In both Figs. 14 and 15, $\overline{Q}_{xw2} \approx \overline{Q}_{xw1}$ for high $Da = 0.1$ for all γ_p conforming to the well noted behavior of porous material filled channel almost behaving like a clear fluid channel at higher values of Darcy number.

Plots of $\overline{Q}_{xw} (= \overline{Q}_{xw1} + \overline{Q}_{xw2})$ vs. X^* for $\gamma_p = 0.2$, 0.4, 0.6 and 0.8 are shown in Fig. 16(a–d). $\overline{Q}_{xw}$ reaches unity for $X^* > 0.2$, indicating that the fluid got heated (or cooled) from T_e, the entry temperature to the T_w, the wall temperature. Fig. 16(a–d) depict the total heat transferred from the two walls to the fluid for different porous fractions, whereas Figs. 14 and 15 are useful in obtaining the heat transferred from each wall separately.

It is easy to verify from Figs. 8 and 9 and Fig. 16(a–d) that, $\overline{Q}_{xw} = \overline{Q}_{xf} = (1 - \theta^*)$. It is noted that this equality may not be valid always, for example, when viscous dissipation is included.

5.8. Net change in total heat transfer and optimal porous insert

5.8.1. Optimum based on net change in wall heat transfer

In this section, whether providing a porous insert enhances the wall heat transfer or not is examined. The net improvement in wall heat transfer, $\Delta\overline{Q}_{xw}$, is defined as the difference between the heat transferred from both the walls when the porous layer is attached and the heat transferred in the case of a clear fluid channel. $\Delta\overline{Q}_{xw}$ is given by,

$$\Delta\overline{Q}_{xw} = \overline{Q}_{xw1}|_{\gamma_p} + \overline{Q}_{xw2}|_{\gamma_p} - 2\overline{Q}_{xw}^{\gamma_p=0}|_{\gamma_p=0} \tag{39}$$

Plots of $\Delta\overline{Q}_{xw}$ vs. porous fraction, γ_p for $Da = 0.001$, 0.005, 0.01 and 0.1 at five axial positions, $X^* = 0.001$, 0.005, 0.01, 0.05 and 0.1 are shown in Fig. 17(a–e) respectively. The following features are evident. a) $\Delta\overline{Q}_{xw} < 0$, for $\gamma_p < 0.5$, i.e., insertion of a porous layer does not enhance the heat transfer until $\gamma_p > 0.5$ approximately.

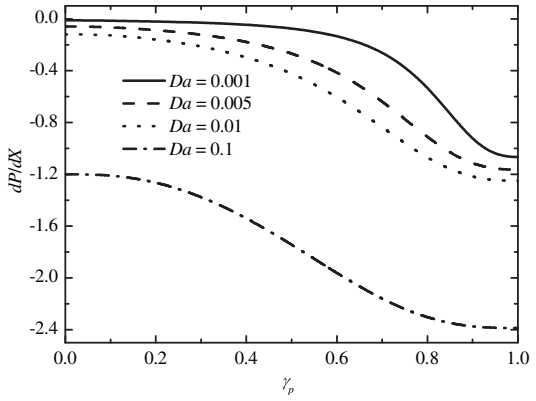

Fig. 18. Variation of pressure gradient with porous fraction for different *Da*.

b) $\Delta\overline{Q}_{xw}$ is minimum when $\gamma_p \approx 0.25$. c) $\Delta\overline{Q}_{xw}$ attains a maximum at $\gamma_p \approx 0.8$. This value of γ_p interestingly is independent of *Da* and X^*. This feature implies that desired enhancement in heat transfer can be attained with a porous insert of uniform thickness. Further, it is of interest to note that a porous insert of $\gamma_p \approx 0.8$ provides the maximum enhancement in heat transfer, even more than that of a channel fully filled with a porous material. It is obvious that the pressure drop when $\gamma_p = 0.8$, will be lower than that when $\gamma_p = 1.0$.

5.8.2. Pressure gradient variation with porous fraction

A plot of P_{gr} vs. γ_p, is given in Fig. 18. It can be seen that $|P_{gr}|$ is substantially lower for $\gamma_p = 0.6$, or even for 0.8 compared to that for $\gamma_p = 1.0$, particularly for lower *Da*, which are relevant. At higher *Da* > 0.1, it is well known that the porous material filled channel behaves almost like a clear channel. Thus maximum enhancement in heat transfer occurring at $\gamma_p \approx 0.8$ is a distinct advantage in terms of pumping power.

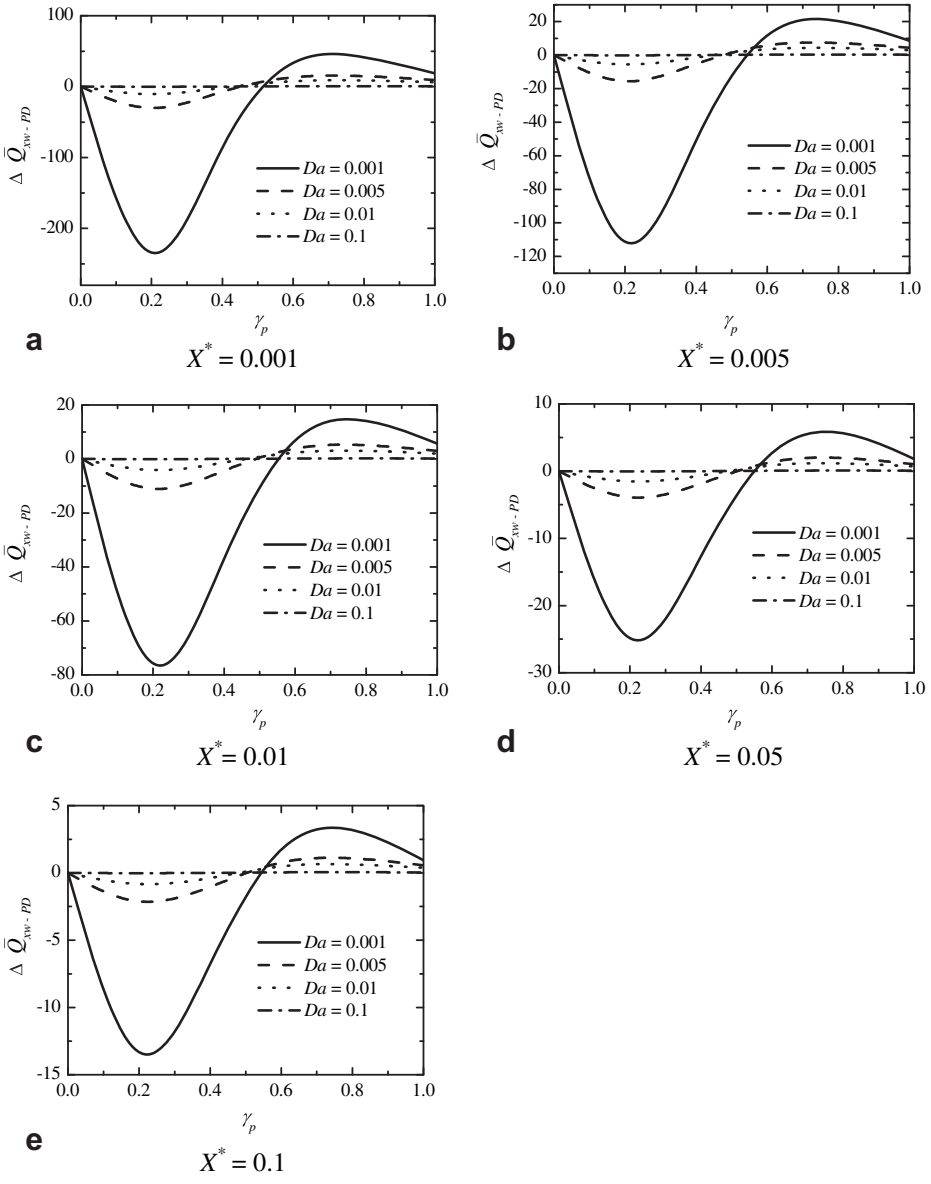

Fig. 19. Variation of $\Delta\overline{Q}_{xw-PD}$ with γ_p for different Darcy numbers, at (a) $X^* = 0.001$, (b) $X^* = 0.005$, (c) $X^* = 0.01$, (d) $X^* = 0.05$ and (e) $X^* = 0.1$.

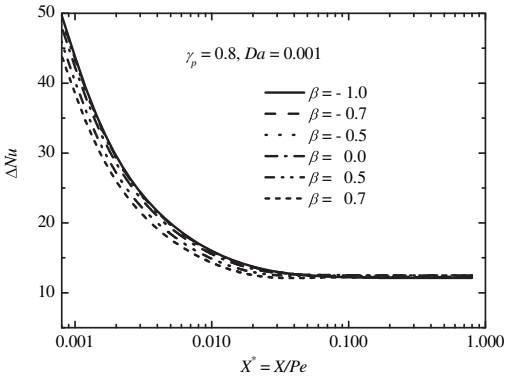

Fig. 20. Variation of ΔNu with X^*, for $Da = 0.001$, $\gamma_p = 0.8$ for different values of stress jump coefficient.

5.8.3. Optimum based on net change in wall heat transfer per unit pressure drop

An alternate way to optimize the porous insert thickness is based on enhancement in heat transfer per unit pressure drop. A quantity, $\Delta\overline{Q}_{xw-PD}$ is defined as,

$$\Delta\overline{Q}_{xw-PD} = \Delta\overline{Q}_{xw}/\left(P|_{X^*=0} - P|_{X^*}\right) \tag{40}$$

It may be noted that the denominator in the RHS of Eq. (40) is nothing but the product of P_{gr} and X^*, where P_{gr} is the non-dimensional pressure gradient given by Eq. (24). Also the denominator in the RHS of Eq. (40) has been written such that the sign of $\Delta\overline{Q}_{xw-PD}$ is the same as that of $\Delta\overline{Q}_{xw}$. Plots of $\Delta\overline{Q}_{xw-PD}$ vs. γ_p for different Da (=0.001, 0.005, 0.01 and 0.1) at $X^* = 0.001$, 0.005, 0.01, 0.05 and 0.1 are given in Fig. 19(a–e).

The qualitative features in Fig. 19 are similar to those in Fig. 17. The maximum $\Delta\overline{Q}_{xw-PD}$ occurs at $\gamma_p \approx 0.7$. The main difference being, $|\Delta\overline{Q}_{xw-PD}| > |\Delta\overline{Q}_{xw}|$ for $\gamma_p < 0.5$ and $|\Delta\overline{Q}_{xw-PD}| < |\Delta\overline{Q}_{xw}|$ for $\gamma_p > 0.5$. This implies that, though the net heat transfer decreases, the additional pressure drop has not been too large for $\gamma_p < 0.5$. Whereas, $|\Delta\overline{Q}_{xw-PD}| < |\Delta\overline{Q}_{xw}|$ for $\gamma_p > 0.5$ indicates that the enhancement in the heat transfer occurs at a relatively higher pressure drop. In addition, it is to be noted that, proper weights for the additional pressure drop and the enhancement in heat transfer need to be taken into account.

5.9. Influence of stress jump condition at the porous–fluid interface

The numerical results so far presented, assumed that the velocity and velocity gradient are continuous at the interface by setting $\beta = 0$, i.e., there is no stress jump. In order to examine the influence of stress jump, the stress jump boundary condition given by Eq. (14) has been incorporated with $\beta = -1.0, -0.7, -0.5, 0.0, 0.5$ and 0.7 in obtaining the velocity profiles. Subsequently, the corresponding temperature profiles and Nusselt numbers have been evaluated. ΔNu which expresses the net change in the Nusselt number due to the porous insert is defined by,

$$\Delta Nu = Nu_{1x}|_{\gamma_p} + Nu_{2x}|_{\gamma_p} - 2Nu^{\gamma_p=0} \tag{41}$$

A plot of ΔNu vs. X^* is shown in Fig. 20 for $Da = 0.001$ and $\gamma_p = 0.8$ for different values of the stress jump coefficient. $\gamma_p = 0.8$ has been chosen since $\Delta\overline{Q}_{xw}$ has been found to be maximum at $\gamma_p \approx 0.8$ for all X^*. ΔNu does not differ significantly with β. Thus, it can be expected that the maximum (or optimum) values of $\Delta\overline{Q}_{xw}$ (or $\Delta\overline{Q}_{xw-PD}$) determined and the corresponding γ_p do not differ much with the stress jump coefficient.

6. Conclusions

Non-dimensional bulk mean temperature has been directly related to the energy gain by the fluid. The thermal field in a channel partially filled with a porous medium also satisfies the fully developed condition, but needs larger axial distance compared to clear channels or those fully filled with porous material. The wall heat transfer on the porous and fluid sides are unequal owing to geometric asymmetry, when the channel is partially filled with a porous insert. Porous inserts of porous fraction less than 0.5 do not lead to an increase in the heat transfer compared to that of clear fluid channel. The maximum enhancement in the wall heat transfer is attained at a porous fraction of, $\gamma_p \approx 0.8$. Maximum enhancement in heat transfer per unit pressure drop occurs at $\gamma_p \approx 0.7$. Relative to a channel fully filled with a porous material, the partially filled channel at a porous fraction of 0.8 or 0.7 has a substantially lower pressure gradient. The effect of stress jump at the interface on optimum porous fraction and enhancement in heat transfer is not significant.

Acknowledgement

One of the authors, D. Bhargavi acknowledges Council of Scientific and Industrial Research (CSIR), India for financial support.

References

[1] R.K. Shah, A.L. London, Laminar Flow Forced Convection in Ducts, Advances in Heat Transfer, Supplement 1, Academic Press, New York, 1978.
[2] M. Kaviany, Laminar flow through a porous channel bounded by isothermal parallel plates, Int. J. Heat Mass Transf. 28 (1985) 851–858.
[3] D. Poulikakos, M. Kazmierczak, Forced convection in a duct partially filled with a porous material, J. Heat Transf. ASME 109 (1987) 653–662.
[4] V.V. Satyamurty, D.R. Marpu, Numerical study of forced convection heat transfer in the developing region of a porous channel, in: Proceedings of V International Symposium on Numerical Methods in Engineering, Switzerland, 1989, pp. 729–734.
[5] G.S. Beavers, D.D. Joseph, Boundary conditions at a naturally permeable wall, J. Fluid Mech. 30 (1967) 197–207.
[6] D.A. Nield, A. Bejan, Convection in Porous Media, third ed. Springer, NewYork, 2006.
[7] K. Vafai, S.J. Kim, Fluid mechanics of the interface region between a porous medium and a fluid layer – an exact solution, Int. J. Heat Fluid Flow 11 (1990) 254–256.
[8] J.Y. Jang, J.L. Chen, Forced convection in a parallel plate channel partially filled with a high porosity medium, Int. Comm. Heat Mass Transf. 19 (1992) 263–273.
[9] J.A. Ochoa-Tapia, S. Whitaker, Momentum transfer at the boundary between a porous medium and a homogeneous fluid: I- theoretical development, Int. J. Heat Mass Transf. 38 (1995) 2635–2646.
[10] J.A. Ochoa-Tapia, S. Whitaker, Momentum transfer at the boundary between a porous medium and a homogeneous fluid: ii- comparison with experiment, Int. J. Heat Mass Transf. 38 (1995) 2647–2655.
[11] A.V. Kuznetsov, Analytical investigation of the fluid flow in the interface region between a porous medium and a clear fluid in channel partially filled with a porous medium, Appl. Sci. Res. 56 (1996) 53–67.
[12] A.V. Kuznetsov, Influence of the stress jump condition at the porous – medium/clear-fluid interface on a flow at a porous wall, Int. Comm. Heat Mass Transf. 24 (1997) 401–410.
[13] A.V. Kuznetsov, Analytical investigation of couette flow in a composite channel partially filled with a porous medium and partially with a clear fluid, Int. J. Heat Mass Transf. 41 (1998) 2556–2560.
[14] A.V. Kuznetsov, Analytical study of fluid flow and heat transfer in a composite channel partly filled with a brinkman-forchheimer porous medium, flow, Turbulence and Combustion 60 (1998) 173–192.
[15] A. Alazmi, K. Vafai, Analysis of fluid flow and heat transfer interfacial conditions between a porous medium and a fluid layer, Int. J. Heat Mass Transf. 44 (2001) 1735–1749.
[16] M.A. Al-Nimr, M. Alkam, Unsteady non-Darcian forced convection analysis in an annuls partially filled with a porous material, Trans. ASME J. Heat Transf. 119 (1997) 1–6.
[17] S. Chikh, A. Boumedien, K. Bouhadef, G. Lauriat, Analytical solution of non – Darcian forced convection in an annular duct partially filled with a porous medium, Int. J. Heat Mass Transf. 38 (1995) 1543–1551.
[18] M. Alkam, M.A. Al-Nimr, Solar collectors with tubes partially filled with porous substrate, Trans. ASME J. Sol. Energy Eng. 121 (1999) 20–24.
[19] M. Alkam, M.A. Al-Nimr, Improving the performance of double-pipe heat exchanger by using porous substrates, Int. J. Heat Mass Transf. 42 (1999) 3609–3618.

[20] M.K. Alkam, M.A. Al-Nimr, M.O. Hamdan, On forced convection in channels partially filled with porous substrates, Heat Mass Transf. 38 (2002) 337–342.
[21] M.O. Hamdan, M.A. Al-Nimr, M.K. Alkam, Enhancing forced convection by inserting porous substrate in the core of a parallel-plate channel, Int. J. Numer. Meth. Heat Fluid Flow 10 (2000) 502–518.
[22] D. Bhargavi, V.V. Satyamurty, G.P. Raja Sekhar, Effect of porous fraction and interfacial stress jump on skin friction and heat transfer in flow through a channel partially filled with porous material, (To appear in) J. Porous Media 13 (Issue 1) (2010).
[23] V.V. Satyamurty, Successive Accelerated Replacement Scheme Applied to Study of Natural Convection Heat Transfer in Porous Cryogenic Insulations Paper no. 85-WA/HT-37, ASME, 1984.
[24] V.V. Satyamurty, D.R. Marpu, Relative Effects of Variable Fluid Properties and Non-Darcy Flow on Convection in Porous Media, vol. 96, ASME HTD, 1988, pp. 613–621.
[25] D.R. Marpu, V.V. Satyamurty, Influence of variable fluid density on free convection in rectangular porous media, Trans. ASME J. Energy Resour. Technol. 111 (1989) 214–220.
[26] V.V. Satyamurty, D.R. Marpu, Influence of linear and non-linear variation of viscosity on free convection in liquid filled rectangular porous slabs, Chem. Eng. Comm. 88 (1989) 173–185.
[27] D.R. Marpu, Studies on Fluid Property Variation and Non-Darcy Flow on Free and Forced Convection in Porous Media, (Ph.D, Thesis), IIT Kharagpur, India, 1990.
[28] R.V. Sharma, Studies on Influence of Fluid Density Variation and Non-Darcy Flow on Natural Convection in a Porous Box, (Ph.D, Thesis), IIT Kharagpur, India, 1998.
[29] Prakash Chandra, Studies on Convection Heat Transfer in Fluid Filled Saturated Anisotropic Rectangular Porous Slab, (Ph.D. Thesis), IIT Kharagpur, India, 2004.
[30] V.V. Satyamurty, Prakash Chandra, Natural convection heat transfer in anisotropic rectangular porous slab subjected to end to end temperature difference, in: Proceedings of 19th National and 8th ISHMT-ASME Heat and Mass Transfer Conference, 3–5 January, 2008, Hyderabad, India (2008).
[31] J. Mitrovic, B. Maletic, Heat transfer with laminar forced convection in a porous channel exposed to a thermal asymmetry, Int. J. Heat Mass Transf. 50 (2007) 1106–1121.